Research Paper

Feasibility of Digital Image Correlation for railroad tie inspection and ballast support assessment.

Alessandro Sabato[1] and Christopher Niezrecki[2]

[1] Department of Mechanical Engineering, University of Massachusetts Lowell, 1 University Avenue, Lowell, 01854 MA, USA.

[1] Alessandro_Sabato@uml.edu

[2] Christopher_Niezrecki @uml.edu

Abstract

Structural health monitoring (SHM) of aging railway tracks is important for safety, to prevent catastrophic failure, and to reduce maintenance costs. The tracks and foundations are complex systems that may contain defects or damage including internal rail cracks, pitting or surface erosion, degradation of ballast support, or railway crosstie-ballast failures. In recent years, interest has grown in performing SHM by measuring structural deformation, full-field strain, and geometry profiles using three-dimensional (3D) Digital Image Correlation (DIC) systems. In this study, a novel approach to use DIC and pattern projection to assess the deformation of railway tracks is proposed. The proposed sensing approach should allow a railcar mounted sensing system to perform interrogation while moving at typical operating speeds (e.g. 60 mph). The feasibility of the proposed 3D DIC system is evaluated through extensive laboratory tests, demonstrating its ability to measure the crosstie's full-field displacement and shape (i.e. at levels similar to what is found in the field) as different loading conditions are applied and taking into account the effect of the strong motion characterizing the railorad service environemtn on the accuracy of the measurements.

Corresponding Author:

Alessandro Sabato, University of Massachusetts Lowell, One University Ave, Lowell, MA, 01854, USA.

Email: Alessandro_Sabato@uml.edu

Keywords

Ballast, crosstie, Digital Image Correlation, railroad, Structural Health Monitoring.

1 - Introduction

Civil engineering structures such as bridges, buildings, tunnels, and railways continue to be used despite aging and deterioration well past their design life. In 2013, the American Society of Civil Engineers (ASCE) rated the state of the U.S. railroads as mediocre, despite the $75 billion USD invested in freight and passenger railways for improving the state of railroad's tracks, bridges, and tunnels since 2009 [1]. Statistics released from the US Federal Railroad Administration (FRA) for the decade 2005-2015 indicated that nearly 25,000 train accidents happened nationwide and that two-out-of-three were derailments that included more than $2.5 billion USD in reportable costs. The same statistics showed that one-out-of-three of the accidents were caused by track failures including rails, crossties, joint bars, and anchoring [2].

The railway is an extremely complex system, which includes rails, railroad ties (or sleepers), fasteners, ballast, and an underlying subgrade (Figure 1).

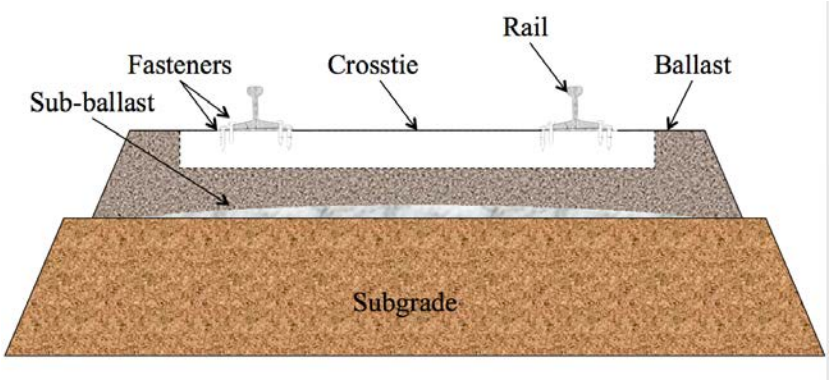

Figure 1. Cross-section of a railroad's components (not to scale).

Each of them have different functionalities, but their conditions all contribute in determining the state of the infrastructure and in assessing the potential risk for train derailments [3]. Rails are the portions of the structure that enable trains to move by providing a dependable surface for their wheels to roll. The standard steel used for their manufacturing is typically constant (Young's modulus: 210 GPa and density: 7850 kg·m^{-3}), while the geometry varies according to the application and the country [4]. Ties' main functions are to: (1) hold rails to maintain gauge and vertical position, (2) receive the load from the rail and distribute it over the supporting ballast with diminished pressure level, and (3) restrain the lateral and longitudinal rail movements [5]. Crossties are made of hardwood timber, because of the lower cost and easier installation, or pre-stressed concrete for improving stability and durability. Steel and plastic composite sleepers are sometimes employed [6]. Fastening systems refers to a number of parts (e.g. screws, elastometric pads, clamps, bolts, etc.) used for securing the rail to the sleepers and prevent any relative motion. The ballast, typically comprising large sized aggregate particles with uniform gradation, is an essential layer in the railroad track substructure. Its functions include: (a) resistance to vertical, lateral, and longitudinal forces to facilitate load distribution and drainage, (b) track resilience and energy absorption, and (c) water drainage [7]. To finish, the subgrade, a highly-variable in composition foundation, supports the ballast and sub-ballast layers under traffic loads [4].

Usually, track failures may happen at different locations. They can interest the wheel-rail interface due to severe contact stresses and induce fatigue cracks [8, 9], or can occur on the tie-ballast interface and imply support and stability failures. In these cases, lack of adequately distributed loads may also lead to deterioration of other parts of the track system, subgrade failure, ballast crushing, ties displacement, insufficient restraint of the rails, rail flaws, and rail breaks [10]. Crossties experience a number of failure modes affecting their in-service performances depending on the material they are made of. Concrete ties are

subjected to flexural cracking [11] on their upper part, which increase the corrosion risk [12], and to abrasion at the ballast interface, which may lead to pulverization [13] and center binding support conditions as happened in 2013 in the case of the freight train derailment in Bronx, NY [14]. The investigations highlighted ballast pulverization phenomena and ties showing different degree of abrasion in the lower part, resulting in portion of the ties still supported by the ballast and others not. This condition causes different tail bending profiles over a long period of time, which increases the derailment risks.

An easy-to-use, effective, and autonomous Structural Health Monitoring (SHM) system for tie-ballast condition assessment, would allow the detection of potentially dangerous situations at an early stage and providing an efficient way to extend the operational life of railway structures, while not interfering with train operations. Since an efficient approach to determine the overall tie deflections is still missing, the FRA is continuing to solicit proposals for developing track inspection technologies that detect ties' vertical deflection and defects before they become failures in service and for expanding the use of automated recording methods to provide more frequent and cost-effective measurements of track and tie-ballast interface conditions [15].

In this study, a novel system for providing accurate in-track measurement of tie deflection profiles using the three-dimensional (3D) Digital Image Correlation (DIC) technique is proposed. In particular, the feasibility of using two or more sets of camera pairs attached to the underside of a rail car to observe a pattern projected on the railway track is discussed in this research. Results of extensive laboratory tests presented in this paper have proven that the 3D DIC system can measure the relative tie deflections over the entire crosstie area (i.e. both inside and outside the rail) with a resolution of 10^{-5} meter and with the same accuracy of a wire-based high-accuracy Linear Variable Differential Transformer (LVDT). Numerous laboratory tests are performed on a track mock-up that possesses crosstie displacement levels similar to what is experienced in the field when a railcar passes over a section of the track. If fully developed, the proposed system could optically

interrogate the crosstie deflection profiles while moving at typical operating speeds (e.g. 60 mph) to predict induced stress/strain, assess the ballast support conditions using the deflection or stress/strain predictions obtained, and enable condition based maintenance instead of scheduled based maintenance, while time consuming and unreliable visual inspection.

This paper is organized as follows: Section II (Sensing techniques for railroads monitoring and assessment) highlights the state-of-the-art of systems for railroad track damage detection followed by description of the theoretical foundation of the technology in Section III (Three-dimensional digital image correlation technique). A detailed description of the proposed system is given in Section IV (Experimental test setup). The results of experiments performed on a lab-scale railroad track mock test, together with a quantitative comparison of the 3D DIC system with wired displacement sensors, are presented in Section V together with an evaluation of the effect of vibrations on the accuracy of the measurements (Analysis of the results). Finally, conclusions are drawn and future work is briefly outlined in Section VI (Conclusions). This paper represents the first research study to investigate the feasibility to use DIC and pattern projection as a means to measure track deflection profiles for the purpose of assessing crosstie and ballast support condition.

2 - Sensing techniques for railroads monitoring and assessment

To improve the quality of railroad track health monitoring data, more advanced measurement techniques have been implemented in the last decades. In this section a review of recent research for railroad SHM is presented with emphasis on that focusing on the tie-ballast assessment. Strain gauges and accelerometers are the most commonly used sensors. Strain gauges are usually deployed in the rail foot or web and are used for measuring the load at the rail head to estimate the wheel-rail bending forces [16]. To generate accurate results, the track properties, geometrical characteristics, and dynamic parameters must be

well known. Also, another drawback of this technique concerns the disposition and the high number of gauges to be deployed to obtain high-quality measurements with appreciable spatial resolution. Some research suggests the use of eleven strain gages on each rail [17], while others propose systems made of eight gauges placed on the rail neutral axis as the best compromise between measurement sensitivity and deployment [18]. As it is possible to observe and to completely characterize a small section of a railroad track, a very large and impractical number of gages are required to monitor a length of track of any appreciable length, which increases deployment costs and installation time for large-scale monitoring. Currently, railroad track management companies employ strain gauges as sensing elements in the Truck Performance Detector (TPD) for measuring lateral and vertical forces during the negotiation of a curved portion of the track [19]. To finish, the use of optical Fiber Bragg Grating (FBG) strain sensors is taking hold for monitoring the condition of critical components of track, rail, and wheel and for identifying features indicative of changes [20, 21]. Although these sensors can measure relatively long lengths (~1 km), the instrumentation and installation is still expensive and not effective for monitoring throughout an entire railway. Accelerometers have proven to be reliable and easy-to-install sensors for detecting dynamic forces at the wheel-rail interface, which can cause damages to track components and rolling stock axle bearings [22]. They can be used for evaluating the state of the track from the amplitude of the measured accelerations evaluating tie-ballast gaps using tie-mounted accelerometers and rail-tie gaps using rail-mounted sensors [23]. Accelerometers also can be used for determining the rails' displacement when loaded statically or in operation. However, this computation is not always accurate because of the numerical errors introduced by the double integration of acceleration data performed to compute the displacements [24]. For achieving these results, several studies presented in the literature employed from two to 21 accelerometers to cover a distance up to 12 meters [16, 25], demonstrating that this technique is time consuming and allows for obtaining information at only a few discrete points.

Other techniques used for monitoring the railway track health, consists of the use of impedance-based damage detection approaches using piezoelectric [26] and wireless macro-fiber composite (MFC) [27] transducers. These systems utilize the direct relationship between the mechanical impedance of the track and electrical impedance of the bonded transducer. Both systems showed some drawbacks and instability in the measured data caused by changes in the environmental or operational conditions (e.g. temperature, humidity, external loadings, or sensor bonding conditions), which limited their applicability for long-term monitoring. Due to the fast development of Wireless Sensor Networks (WSN), other wireless systems were proposed for remote monitoring of track infrastructures and carriages by developing sensor nodes embedding different sensing elements (e.g. displacement transducers [28], gyroscopes [29], inclinometers [30], strain gauges [31], temperature sensors [31]) [32].

Conventionally, measurements performed using contact-type sensors are time consuming and can provide data only at discrete locations. Moreover, these sensors are usually wired to a data acquisition and a power supply, which makes the set-up cumbersome and costly. Recent technological developments have made non-contact measurements extremely appealing tools for SHM. For instance, recent improvement in the active and passive infrared (IR) images allowed detecting the presence of anomalies from the change in IR emission of the rail surface as changing stress conditions are applied (i.e. wheel passage and unloading phases) [33, 34]. Nevertheless, the power demanding and the sensitivity of this method to changes in boundary conditions (e.g. surface cleanliness, difficulty in detecting low emissivity materials, presence of grease and dirt, etc.), made IR imagining still inadequate for large-scale track monitoring. Another technique experiencing increasing popularity is the Ultrasonic Testing (UT), which is based on the propagation of waves having frequency in the 50 kHz - 1 MHz range to detect rail defects [35]. Due to lack of accuracy of the UT

technique in detecting some particular defect [36] and limited speed inspection [37], novel inspection methods such us the guided waves were developed for coupling those problems [38].

With particular reference to tie-ballast and substructures assessment, other non-contact measurement techniques have been proposed. For instance, Ground Penetrating Radar (GPR) has shown the ability to map concrete and wood crossties as well as ballast shoulders conditions using a 1 GHz radar [39]. Nevertheless, the resolution of this system, because of the relative similarity of concrete and ballast properties, makes it difficult to distinguish the boundaries of the two components. As a matter of fact, the GPR currently allows obtaining qualitative indications only, while for quantitative data on damage and defects, further improvements needs to be achieved [40].

Advancements made in cameras technology, optical sensors, and image processing algorithms made machine vision a technique extremely appealing for tracking surfaces defects, rail and ties profile detection, and ballast condition evaluation [41]. For instance, automated visual inspection made analyses possible as the train moves. A high-speed camera captures images of the track's component and a remote processor analyzes them using machine learning algorithms. By using this technique is possible to evaluate the current state of the infrastructure and compare it with baseline conditions to obtain information about possible surfaces flakes, cracks and groove in the rail head profile [42], percentage of wear [43], moving crossties and absence of ballast [44], and missing bolts [37, 45]. Another potential optical technique used for measuring the condition of railroad track is DIC, which has the potential to measure rail displacements and to evaluate parameters that characterize the track failure mechanism (e.g. stiffness, damping, strain distribution, etc.) One of the first studies performed combined the use of a webcam and a small telescope [46]. Laboratory validation tests performed over three different railway tracks and train speed showed that the video monitoring system could measure the dynamic displacement of the railway track; in particular, peak-to-peak displacements of 0.04 mm and frequencies up to

4 Hz. Another DIC system using four synchronized, 85 mm focal length, high-speed cameras was used to measure the out-of-track motion of the vertical and longitudinal rail displacement using the texture on the rail itself and tie-mounted targets [47]. The cameras were mounted at a fixed position near the track and away from the train. The proposed system was evaluated in two different sites, one with a high-quality subgrade and one with a peat subgrade, during the passage of eleven trains at the monitored location. Data recorded using the four cameras were used to determine the stiffness and damping of the subgrade and to investigate the factors that influence the magnitude of longitudinal rail displacement.

As can be observed several different systems have been proposed for assessing the conditions of various components of the railroad track. What is presented in this section is meant to be a short summary only; for a complete discussion about the currently used SHM methods the interested readers can refer to the papers [48, 49].

3 – Three-dimensional digital image correlation technique

Three-dimensional digital image correlation (3D DIC) is a non-contact, full field, optical measuring technique capable of extracting surface strain, displacement and geometry profiles from images acquired through a synchronized stereo camera system. As shown in Figure 2a a point P on the surface of the target object has coordinate (X_P, Y_P, Z_P) in the global coordinate system X-Y-Z with origin in O. The two cameras have their own coordinate system (x_i, y_i, z_i) with origin in C_i, where i = 1,2 while another plane can be defined that the projection of the point P has coordinate (x_i', y_i', f_i'). This plane, belongs to the image or retinal system R_r which is obtained as z_i is shifted by a distance equal to f_i', so the point has coordinate (x_i', y_i', 0) in the image coordinate system. However, since cameras record intensity data at discrete locations (i.e. pixels), another coordinate system named sensor system (x_s, y_s) is introduced. Therefore, based on the pinhole

camera model, three elementary transformation have to be performed. The first one concerns the global coordinates of a target object to the camera system coordinates; then, the projection transformation into the retinal plane, and for finishing the transformation into the sensor coordinate system in pixel units[50]. To sum up, the position of the point P in the global coordinate system is projected in the retinal plane and measured in the sensor coordinate system as P_1 ($x_{s,1}$, $y_{s,2}$) and P_2 ($x_{s,2}$, $y_{s,2}$). Then by combining those two points with the intrinsic and extrinsic parameter of the two cameras, a 3D coordinate of the physical point P can be obtained using triangulation theory [51].

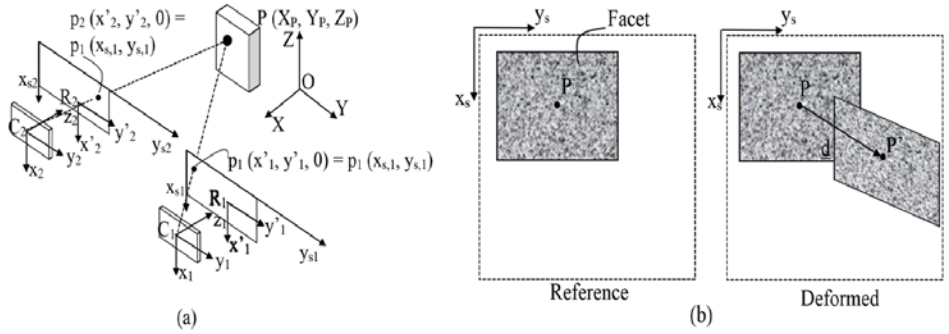

Figure 2. Schematic of stereo imaging setup for DIC: (a) reference planes and pinhole camera model transformations and (b) facets displacement vector.

To perform these measurements, a stochastic pattern (e.g. black and white dots) and/or optical targets are applied to the surface of interest and the relative position of each of them is tracked as the surface deforms over time. By processing the initial pair of images a set of unique correlation areas (i.e. facets) is defined across the measuring area. Facets are usually 5-20 pixel square; thus, it includes several dots of the pattern. The center of each facet is a measurement point that can be thought of as the edge of an extensometer. The position of these facets is tracked through each of the successive acquired images and the 3D coordinates of the entire area of interest are calculated with sub-pixel accuracy [52]. As can be intuited, the basic principle of

DIC is to match the same physical point between a reference image and several deformed stages based on gray-scale variations of continuous patterns. This process is shown in Figure 2b for an easier understanding. Here, a square facet is used as a reference image, while a correlation function is used for searching the corresponding facet and defining a displacement vector $\underline{d}$ [53 - 55]. The correlation algorithm is based on the tracking of the grey value pattern in small local neighborhood facets.

Prior to performing stereo-photogrammetry type measurements, the position of the cameras relative to each other and the distortions of the individual lenses must be determined. To obtain this information a calibration has to be performed by taking several images of an object containing coded optical targets whose positions are previously well-known. With reference to the case of study analyzed in this research, the pair of cameras detect the relative position of each of the dots used for patterning the crosstie; then, stereophotogrammetry techniques are used triangulating the 3D coordinates of each point in the recorded and correlation algorithms are used for calculating their displacement and associated strain [56]. As a projected pattern is used instead of a painted one, the method used for evaluating the displacement is exactly the same. The cameras detect the relative position of each point in the 3D space and use the same algorithms for calculating their relative motion as the target object is deforming. The only difference with the painted case is that in not possible to evaluate the strain of the surface as the pattern is no more supportive with the structure. Developments in optical techniques have made DIC systems a reliable option for SHM measurement on civil and mechanical engineering structures [57 - 60].

4 - Experimental test setup

Within this work, the possibility to develop a 3D DIC system to monitor the tie deflection profiles from a full-size rail car is investigated. For doing this, a wooden full-scale model representing a section of a

railroad track has been built and instrumented as shown in Figure 3. Geometrical dimensions of the mock-test are equivalent to those of a real railroad (ties spacing equal to 0.315 m, rails distance equal to 148.50 m, and crossties dimension equal to 0.235 x 0.019 x 2.590 m,), while the only difference is the crossties depth, which is considerably smaller than that of a real-world tie (i.e. 0.178 m). Thinner ties have been selected to allow them to experience the same vertical deflection characterizing real-world ties (i. e. displacement ranging from $1 \cdot 10^{-3}$ to $8 \cdot 10^{-3}$ m) [61] without having the necessity to apply extremely heavy loads (e.g. on the order of 10^2 kN).

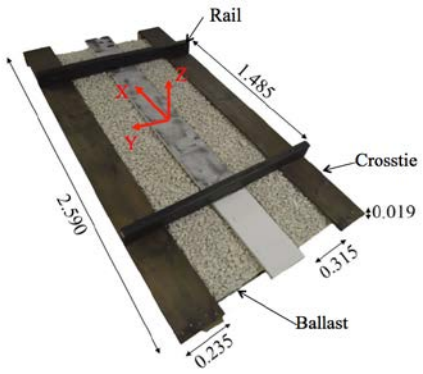

Figure 3. Mock-test experimental setup, coordinate system, and dimensions in meters.

The DIC system selected consists of a pair of 2 Megapixel FWX201 series digital cameras manufactured by Baumer GmBH employing a 1/1.8" interline progressive charge coupled device (CCD) monochrome image sensors with a resolution of 1626 x 1236 pixels and a pixel size of 4.4 x 4.4 10^{-6} m [62]. The cameras were fitted with 8.5 mm focal length lenses manufactured by Edmund Optics Ltd. The 3D DIC system was positioned to have a working distance of 1 meter, a base distance of 0.68 m, and a 36.5° separation angle between the cameras' central line of sight. In this configuration, the stereo-photogrammetry system was capable of measuring a volume of 0.810 x 0.670 x 0.670 m. While 0.810 m represents nearly the

56% of the distance between the two rails, the depth of the field of view makes it possible to measure out-of-plane displacement up nearly half meter. The decision to use this working distance depends on the features of the train cars commonly used, which is an important geometrical limitation for future measurements. In particular, because of the wheel dimensions (diameter between 0.80 and 0.90 m), it was assumed that a space of nearly one meter is available below each train car to mount the cameras. A wider field of view could be achieved by using smaller focal length lenses, but images distortion may increase in the peripheral areas lowering the resolution of the calculated data. To process the recorded images, the Aramis™ software developed by GOM was used. The setup parameters used in the analysis are summarized in Table 1.

Table 1. Setup parameters used for compute the displacements.

Facets		Filtering		Computational parameters		Deviation	
Size (pixel)	15 x 15	Type (-)	Median	Accuracy (-)	0.040	Calibration (pixel)	0.029
Step (pixel)	13 x 13	Run (-)	5	Residual (-)	20.000	Scale (mm)	0.006
Mode (-)	Rectangular	Size (-)	3	Angle variance (°)	-32.8/45.1	Intersection (-)	0.300

The long-term goal of this research is to develop a 3D DIC system that could be installed underside of a rail car and monitor the tie deflection profiles while operating at full speed. In particular, one set of cameras would be located close to the rail car wheels to detect displacements due to loading, while another set would be located away from the wheels (e.g. ~5 meters) to measure the tie profile under unloaded conditions. At any measurement location along the railcar, the proposed system could possess two pairs of cameras both inside the outside the rail to measure displacements over the entire length of the tie. In addition, since the field of view of the inner pair of cameras cannot cover the whole length of the tie for geometrical constrictions, another pair of cameras could be used to obtain a wider field of view by stitching together the recorded images or by using a wide angle lens. Other research performed have shown that combining images recorded

using adjacent sets of cameras is possible to obtain measurements over wider areas [63, 64]. With reference to the railroad monitoring, it has been shown that by using four sets of cameras it is possible to cover the whole length of the crosstie. Results shown that the stitching process increase the noise floor of the measurement, but makes it still possible to measure displacement on the order of 10^{-4} m [65, 66]. It is expected that a fully developed system, employing high resolution cameras (e.g. 12 Megapixels), would be able to measure the relative tie deflections over the entire tie area (i.e. both inside and outside the rail) with a resolution of approximately $5 \cdot 10^{-6}$ m.

The DIC technique requires the structure under test to either have discernable features or a pattern applied to the surface for pattern matching to occur between both cameras. Furthermore, since patterning each tie on a railroad track is not a practical option, a projector is proposed create the pattern necessary for the DIC system. By using a projected pattern, it is possible to obtain distributed surface geometry for the object being tested. Figure 4 shows the concept of the setup proposed in this research.

Figure 4. Concept setup of a stereo-photogrammetry system and projector that can be used to observe the tie deflection profiles attached to the underside of a rail car (not to scale).

It should be noticed that the system expects the installation of a shroud mounted to the rail car. This feature will help reducing the influence of external lighting on the measurements. Indeed, it is planned to use a set of lamps deployed underneath the car (not shown in Figure 4 for clarity reasons) for providing a constant illumination to the target object. It has been shown that artificial monochromatic light can help obtaining high-quality images suitable for high fidelity deformation measurement [67]. Furthermore, the presence of artificial light facilitates the reduction of the cameras' shutter time and helps preventing from obtaining blurry images useless for measurement purposes.

To validate the performance of the proposed system, different center binding conditions were simulated on the middle tie of the setup shown in Figure 4. In real-world scenarios, the mechanism for center binding begins as the support of ballast under the crosstie is initially concentrated at the rail-seat rather than uniformly distributed. Over time as the cyclic loading of the vehicles is applied, the depression and abrasion of the ballast is most severe under the rail-seat area of the crosstie. As a result, firm support of the ballast is only provided at the center of the crosstie, while it cantilevers over its two ends [68]. This phenomenon is acknowledged as a high-risk failure mechanism [12, 13].

Figure 5. Different center binding conditions simulated during the performed experiments (not to scale).

In the performed experiments, to simulate different ballast conditions, the position of a support placed underneath the central tie was modified as shown in the diagrams shown in Figure 5. The deflected tie shapes may be calculated from the classic beam theory (e.g. Euler-Bernoulli beam or Timoshenko beam) and an appropriate foundation model (e.g. Winkler or Pasternak), but it is beyond the aims of this paper [69, 70]. In particular, condition (a) represents a situation in which the ballast reacts in a uniform manner to the applied loads, while conditions (b) and (c) simulate two different center binding conditions by means of a support placed in different positions below the crosstie.

5 - Analysis of the results

To demonstrate the feasibility of the 3D DIC system described in the previous section and validate the accuracy of the recorded measurements, two different sets of tests were performed. In all of them, to simulate a train transit, fourteen static loads from zero to 510 N (114.65 lb_f) were applied with 39 N (8.77 lb_f) increments to the central tie in correspondence of the two rails (i.e. nearly 0.74 m from the tie's middle point).

During the first experiments the cameras were used for capturing images of the central tie's middle point and tracking the relative displacement of a pattern painted on the tie itself as different loading conditions were applied (Figure 6a). Speckles with a diameter of nearly $3 \cdot 10^{-3}$ m were used to obtain dots having dimension between five and seven pixels in the recorded images (Figure 6c). The goal of this test was to prove that the 3D DIC system was able to detect changes in the crosstie's shape and its full-field displacement for levels commensurate to that found in the field [61, 68]. To achieve a variety of deflections, the beam representing the crosstie was subjected to a variety of incrementally applied loads and boundary conditions. In the second set of experiments, the cameras were moved to the edge of the tie (Figure 6b), but at this time the pattern was projected on the tie using a video projector (Figure 6d).

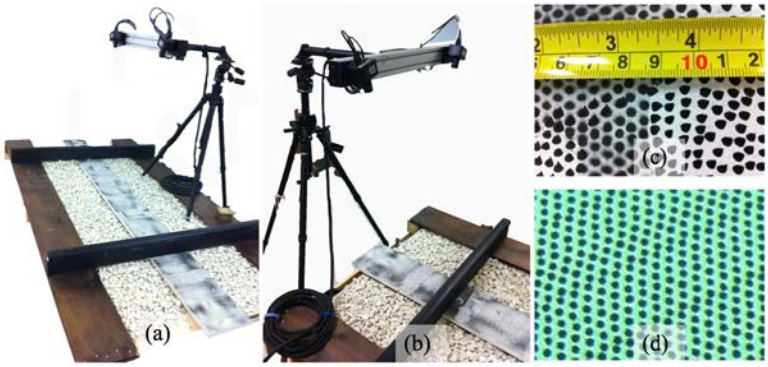

Figure 6. Experimental setup for measurements performed (a) in the middle part of the tie, (b) at its far end. Detail of the (c) painted and (d) projected speckles used for displacement evaluation.

Deflection shapes and full-field displacements were measured; moreover, to prove the accuracy of the recorded data back-to-back comparisons with a Linear Variable Differential Transformer (LVDT) placed below the tie were performed. The objective of this test was to prove that that no significant differences exist when a projected pattern is used compared to a painted one.

5.1 - Experiments performed using a painted pattern

The first test performed consists of loading the tie and measuring the out-of-plane displacement (i.e. vertical displacement Z) and the deformation of the tie's longitudinal section as the load increases from zero to 510 N. For each loading condition, five snapshots were taken to prove measurements repeatability and to allow data averaging during post-processing analyses. Frame rates characterizing high speed cameras (e.g. 100 frame per second), would make the acquisition of such number of images of a specific spot a trivial issue even if the acquisition is performed at full train speed (e.g. 60 mph). The loading curve was repeated for all three simulated center binding conditions. It should be noticed that the first five images recorded in each test refer to the unloaded condition and were used to evaluate the measurement's noise floor. Figure 7 shows the

average in false colors of the full field out-of-plane displacement noise floor measured for the three simulated conditions superimposed to the picture recorded using the left camera, while the upper and the lower values computed in each of the stages are summarized in Table 2. As observed, noise floor range is [+0.0119 to -0.0109] mm, consistent with the theoretical values predicted using the cameras' specifications.

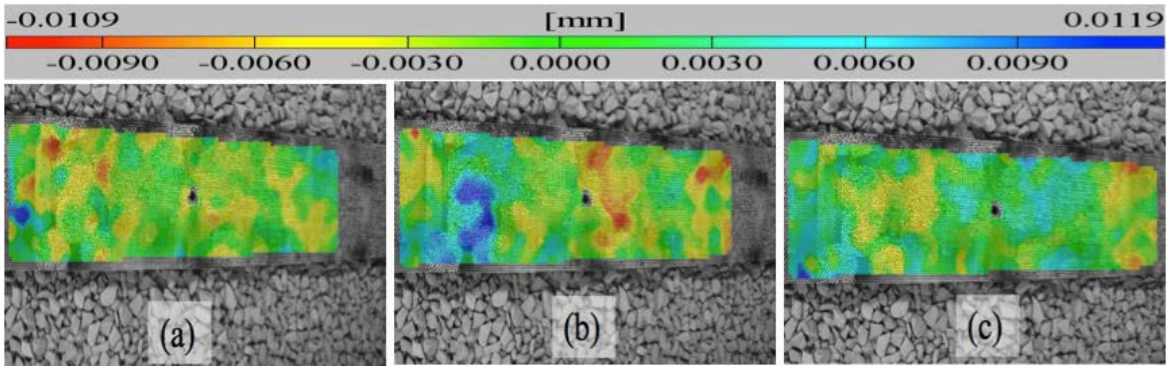

Figure 7. Out-of-plane displacement noise floor for the three boundary conditions (a), (b), and (c) as described in Figure 5.

Table 2. Measured out-of-plane displacement noise floor.

		Image 1	Image 2	Image 3	Image 4	Image 5	Average
Condition (a)	Z_{max} (mm)	0.0063	0.0068	0.0073	0.0068	0.0079	0.0070
	Z_{min} (mm)	-0.0095	-0.0076	-0.0095	-0.0090	-0.0102	-0.0092
Condition (b)	Z_{max} (mm)	0.0193	0.0171	0.0126	0.0121	0.0232	0.0169
	Z_{min} (mm)	-0.0163	-0.0064	-0.0145	-0.0103	-0.0133	-0.0122
Condition (c)	Z_{max} (mm)	0.0103	0.0094	0.0133	0.0119	0.0144	0.0119
	Z_{min} (mm)	-0.0176	-0.0085	-0.0102	-0.0101	-0.0105	-0.0114

The 3D DIC system has been employed to measure the full-field vertical displacement Z experienced by the tie as increasing loads are applied to the rails. To validate the accuracy of the measured displacements, a back-to-back comparison with a LVDT sensor has been performed by comparing the discrete displacement recorded from the images in the position where the transducer was positioned, in the middle of the crosstie

nearly 0.75 m away from the rails. The LVDT transducer was calibrated prior the test and its accuracy was verified by measuring well-known displacements double-checked using a high-accuracy caliper. Tests were performed by loading the tie from 0 to 510 N in correspondence of the two rails and for all of the three center binding condition shown in Figure 5. Figure 8 shows the vertical displacement Z of the selected point measured using the 3D DIC system (lines) and the LVDT (dots) plotted against the applied loads.

Figure 8. Comparison of the vertical displacement Z of a single point measured using the 3D DIC system and a LVDT for all three boundary conditions a, b, and c.

As shown in the figure, an excellent agreement between data recorded using the two systems is observed. In particular, the maximum error is equal to 3.59% (condition c, DIC = -0.860 mm; LVDT = -0.890 mm). The 3D DIC is then used for evaluating the full-field displacement experienced by the crosstie as a load is applied. Figure 9 plots the full-field vertical displacement values for loading increase from 0 to 510 N in false colors superimposed on the images captured using the left camera. In this paper only results regarding the center binding condition (c) are reported for the sake of brevity, but comparable results were obtained for measuring the out-of-plane displacements for the other two center binding conditions as well.

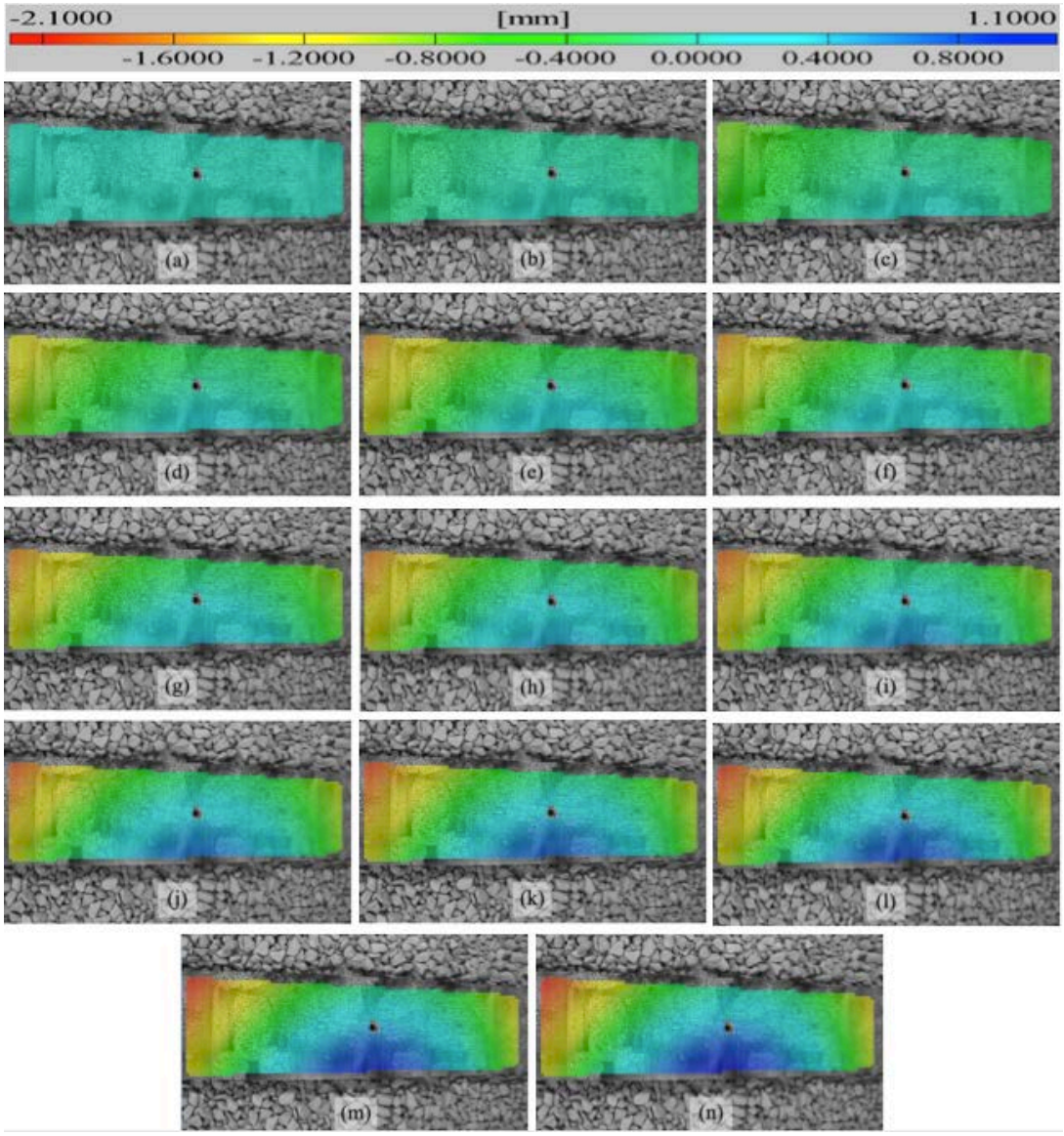

Figure 9. Full-field vertical displacement Z for the boundary condition (c) as function of load increase: (a) 0 N, (b) 39 N, (c) 78 N, (d) 118 N, (e) 157 N, (f) 196 N, (g) 235 N, (h) 275 N, (i) 314 N, (j) 353 N, (k) 392 N, (l) 431 N, (m) 471 N, (n) 510 N.

It is observed that as the load increases, the middle part of the tie raises from nearly $-0.10 \cdot 10^{-3}$ m for the 39 N case to nearly $+0.80 \cdot 10^{-3}$ m for the 510 N load. This displacement is maximum where the support is located, while it is minimum at the tie's two free edges. These results confirm that the crosstie behaves as two cantilever beams at its free edges as firm ballast support is provided in the center only. This is even more evident as an analysis of the tie's longitudinal section is performed. As shown in Figure 10, using the data recorded with the 3D DIC system it is possible to plot the vertical displacement of the tie through the whole cameras' field of view as loads increase.

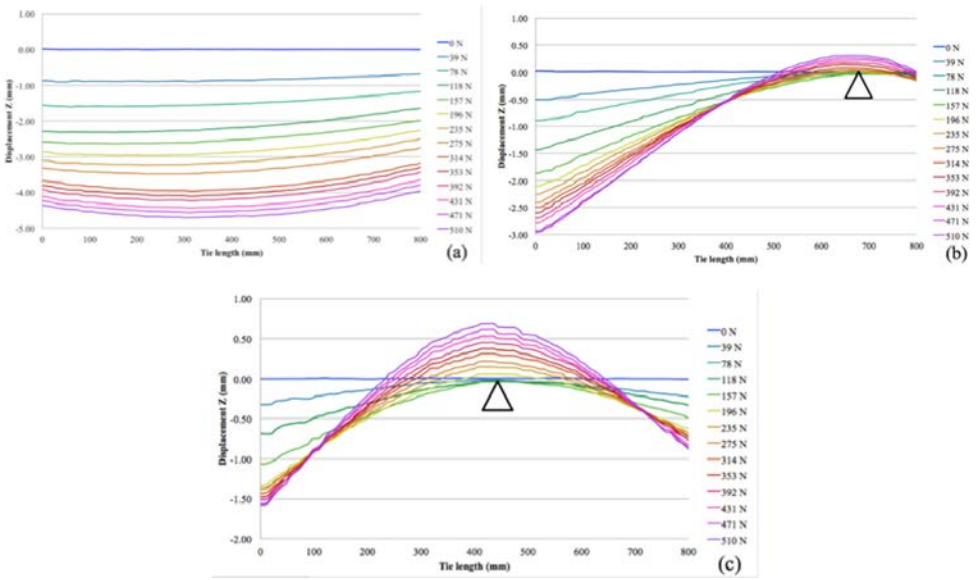

Figure 10. Tie longitudinal profiles as function of the applied loads for the boundary conditions (a), (b), and (c) shown in Figure 5.

This operation is possible by just processing information from pictures, with no need to deploy large array of sensors underneath the tie being tested, demonstrating that the 3D DIC system can easily expedite the monitoring process and is able to extract information throughout the field of view and not just at discrete

points. As observed from data plotted, different center binding conditions result in different tie's longitudinal profiles. Furthermore, the system has shown to be capable of detecting displacements as low as $\pm 10^{-4}$ m.

The 3D DIC measurement makes it possible to easily detect the onset of critical deflections. The results indicate that when the tie is loaded with 510 N are plotted together for the entire simulated center binding conditions, the difference in full field displacement and longitudinal profile are easily detectable.

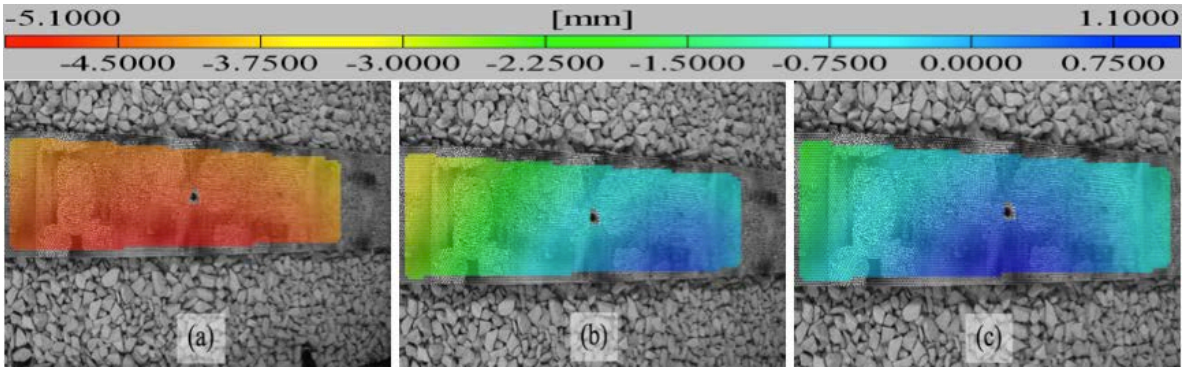

Figure 11. Full-field vertical displacement Z for the boundary conditions (a), (b), and (c) shown in Figure 4 at the maximum applied load.

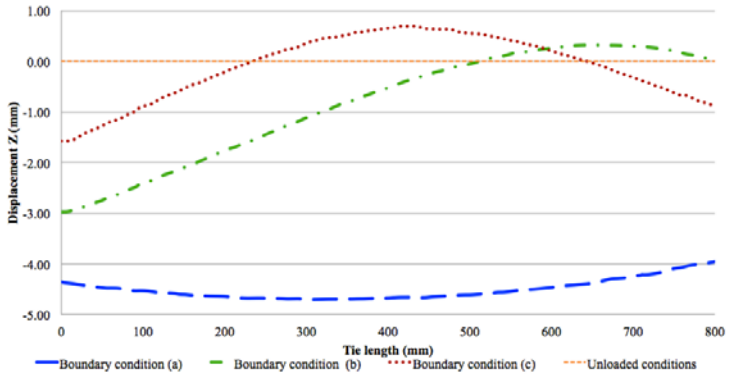

Figure 12. Tie longitudinal profiles for the boundary conditions (a), (b), and (c) shown in Figure 5 at the maximum applied load.

When the tie is not supported, it experiences a subsidence as the load increases. In particular, lower values were measured in the middle part and were equal to $-4.70 \cdot 10^{-3}$ m (Figure 12a). Opposite behavior is highlighted as the tie was supported. The tie experiences the highest profile position where in the support is located ($+3.20 \cdot 10^{-3}$ m and $+6.90 \cdot 10^{-3}$ m for the condition (b) and (c) respectively), highlighted in Figure 12b and 12c by the dark blue areas. On the other hand, the crosstie experiences a negative displacement at its free edges ($-2.97 \cdot 10^{-3}$ m and $-1.58 \cdot 10^{-3}$ m for the boundary condition (b) and (c) respectively), highlighting an absence or a defect in the ballast conditions.

5.2 - Experiments performed using a projected pattern

This experiment is very similar to that described in above paragraph with the difference being that the pattern used for evaluating the 3D displacement was projected on the tie and was not adhered to the tie. As was previously performed, the noise floor was evaluated by taking five snapshots of the three simulated center binding conditions as no load was applied to the tie.

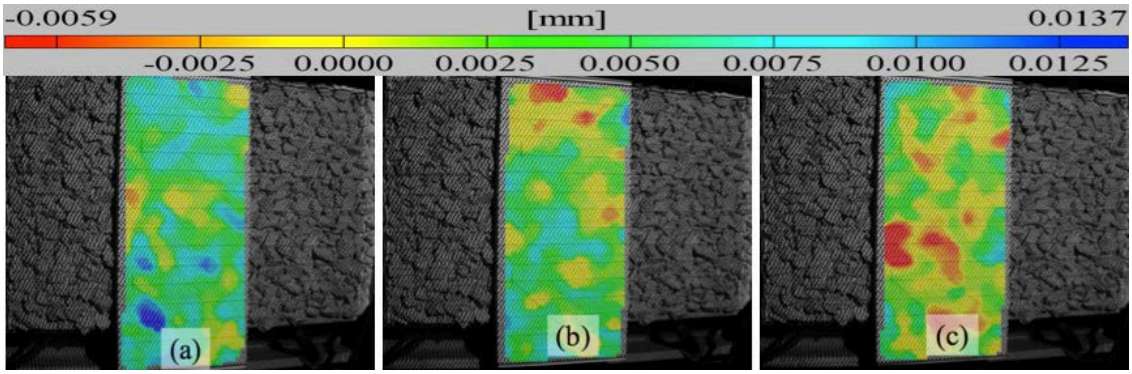

Figure 13. Out-of-plane displacement noise floor for the three boundary conditions (a), (b), and (c) described in Figure 5.

Table 3. Measured out-of-plane displacement noise floor.

		Image 1	Image 2	Image 3	Image 4	Image 5	Average
Condition (a)	Z_{max} (mm)	0.0133	0.0145	0.0142	0.01422	0.0138	0.0140
	Z_{min} (mm)	-0.0098	-0.0025	-0.0031	-0.0071	-0.0063	-0.0057
Condition (b)	Z_{max} (mm)	0.0172	0.0117	0.0116	0.0087	0.0122	0.0122
	Z_{min} (mm)	-0.0082	-0.0063	-0.0086	-0.0094	-0.0070	-0.0079
Condition (c)	Z_{max} (mm)	0.0087	0.0177	0.0194	0.0190	0.0096	0.0148
	Z_{min} (mm)	-0.0086	-0.0009	-0.0014	-0.0000	-0.0092	-0.0040

The average in false colors of the full field out-of-plane displacement noise floor measured superimposed to the picture recorded using the left camera and the upper and the lower values computed in each of the stages are shown in Figure 13 and Table 3 respectively. As observed, noise floor range is [+0.0137 to -0.0059] mm, and on the same order of magnitude of that evaluated for the painted pattern case. To validate the accuracy of the 3D DIC measurements performed using a projected pattern, a direct comparison with those recorded as a painted pattern is employed was performed. Figure 14 plots the longitudinal profiles measured when the two different patterning techniques are employed as the center binding condition (c) is simulated on the crosstie for increasing loads.

Figure 14. Direct comparison for the out of plane displacement measured by the optical system on a longitudinal section of the crosstie when projected and painted patterns are employed.

No significant differences were observed when a projected pattern is used instead of a painted one. Nevertheless, to further validate the accuracy of the measurements performed using the proposed 3D DIC systems when a projected pattern is employed, a back-to-back comparison with a LVDT sensor has been performed. Similarly to what shown in the previous paragraph, a comparison of the discrete displacement recorded from the images in the position where the transducer was positioned was performed. Tests were performed by loading the tie from 0 to 510 N in correspondence of the two rails and for all of the three center binding condition shown in Figure 5 and the LVDT was placed below the left edge of the tie nearly 0.40 m away from the rail. Figure 15 shows the relative position of the selected point measured using the 3D DIC system (lines) and the LVDT (dots) plotted against the applied loads.

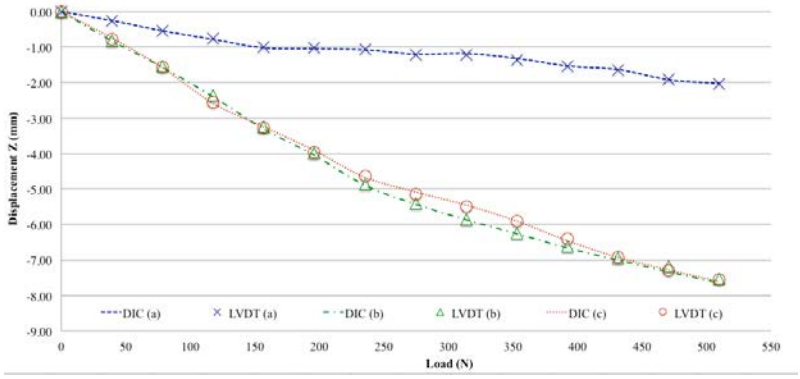

Figure 15. Comparison of the vertical displacement Z of a single point measured using the 3D DIC system and a LVDT for all three boundary conditions a, b, and c.

As shown in Figure 15, there is excellent agreement between data recorded using the LVDT and the DIC system. In particular, the maximum error is equal to -2.62% (condition a, DIC = -0.781 mm; LVDT = -0.762 mm), on the same order of magnitude of the noise floor of the optical system. This implies that DIC can measure the relative displacement of a point with the same accuracy of a high sensitivity, wire-based, LVDT

sensor from images over a wide area, a further demonstration of the validity of the proposed approach. The proposed system has proved to be able to detect displacement as low as 10^{-4} m even when a projected patter is employed. From an analysis of data reported in Figure 16, it easy to observe the different displacements experienced by the tie as a result of the different supporting conditions.

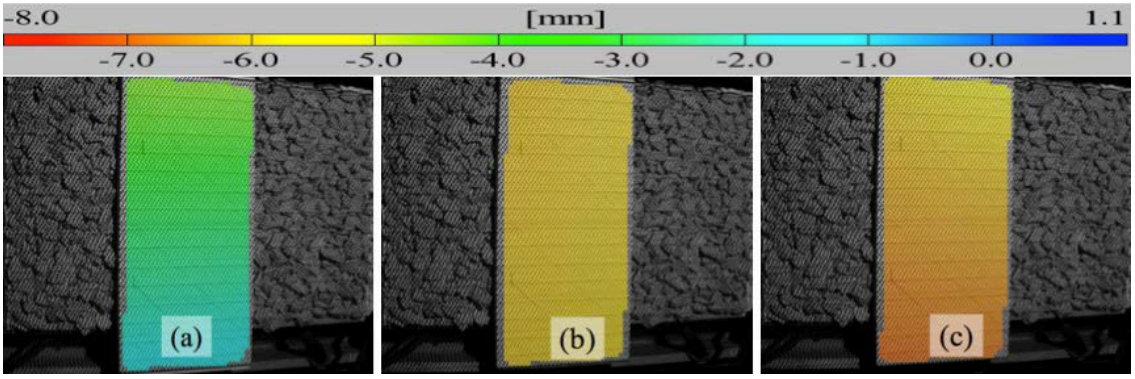

Figure 16. Full-field vertical displacement Z for the three boundary conditions shown in Figure 5 for the maximum applied load measured at the tie's edge.

In particular, as observed in Figure 16a, the crosstie's far edge tends to rise, while the edge close to the rail lowers of nearly $3 \cdot 10^{-3}$ m compared to the unloaded conditions. On the contrary, ties experiencing severe center binding conditions have an opposite behavior, with different level of deflection at their far edge (e.g. on the order of $-7 \cdot 10^{-3}$ m for the tie in Figure 16c).

5.3 – Effect of vibration reduction on the images resolution

Railroads are characterized by strong motions and vibrations. Therefore, it is plausible to expect some variations in the accuracy of the optical-based measurements as the DIC system is operating in railroad service environments. For this reason, the feasibility of a method for vibration compensation is investigated in this paragraph. In particular, the main idea is to develop a damping system which can reduce the vibrations

having frequency higher than a fixed threshold transmitted from the train to the cameras. In particular, the vibration isolation system has been designed for transmitting only low-frequency rigid-body-type motions (i.e. below 2Hz), which can be removed from the images using suitable post processing algorithms [52, 56]. The experimental setup used for validating the robustness of the proposed system is shown in Figure 17.

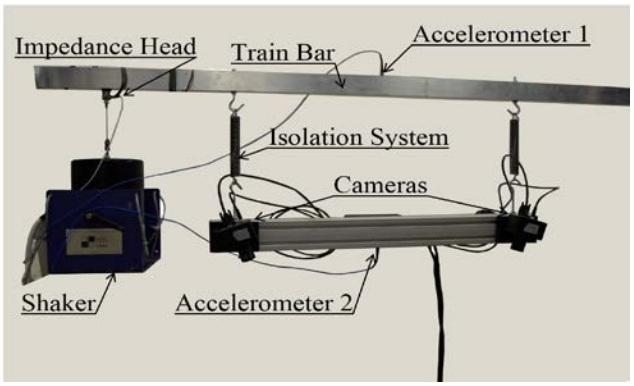

Figure 17. Experimental setup for vibration isolation assessment and image quality determination.

In particular, the shaker shown in the Figure was used for exciting the train bar with a random noise vibration in the range 0 – 40 Hz to simulate the effect of the train motion on the cameras. The camera bar was attached to the train bar by: (a) a spring isolation system and (b) a hard mounted system, while three Integrated Electronics Piezo-Electric (IEPE) sensors where installed at different locations for monitoring the vibration levels. The effectiveness of the isolation system in reducing the vibration transmitted is proved through a series of experimental tests. In the hard mounted case, the equivalent acceleration recorded on the train bar is 2.96 ms^{-2} opposed to 1.71 ms^{-2} measured on the camera bar (i.e. reduction of nearly 42%). On the other hand, the accelerations recorded when the isolation system is installed are equal to 6.62 ms^{-2} and 0.25 ms^{-2} on the train bar and cameras bar respectively, showing that the springs are able to reduce the transmitted vibration by nearly 96% despite the non-optimized system. Similar consideration can be done as the

frequency domain response of the two system is analyzed. In the case of a hard mounted system, the Fast Fourier Transforms (FFTs) of the two signals recorded on the train and camera bars are exactly the same and characterized by the same energy contribution at the different frequencies, while the energy across the excitation frequencies is reduced by nearly 20 dB as the isolation system is installed. The only frequency that does not exhibit a significant reduction in vibration is at 2 Hz, because the natural frequency of the system is 2 Hz.

To validate the performance of the isolation system with regards to DIC measurements, several laboratory tests have been conducted. Tests evaluated the deflection profile of a wooden tie as it was loaded at its two free edges while the camera bar was fixed to the train bar using the two systems shown in Figure 17. A comparison of the results obtained with and without vibration is performed. A confirmation of the quality of the isolation system can be obtained when an evaluation of the tie's longitudinal profile is performed. The shape assumed by the tie is plotted for unloaded and loaded conditions for the three configurations in Figure 18, by averaging and post-processing (i.e. filtering and movement correction) the 10 images recorded for each measurement performed.

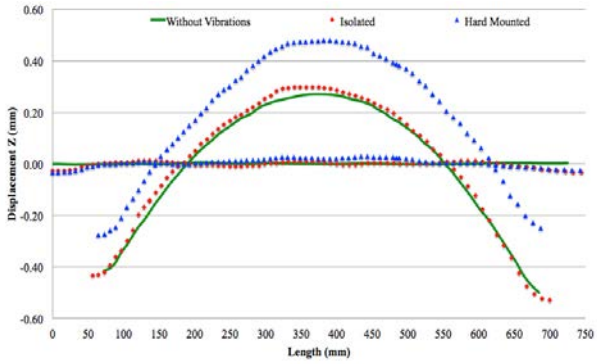

Figure 18. Tie longitudinal profiles as a function of the applied load for the three analyzed configurations.

As observed from the result plotted in Figure 18, no significant differences can be observed when the longitudinal profile measured in absence of vibration is compared to that measured with the 3D DIC system installed with the isolation system. When the hard mounted case is considered, the shape of longitudinal profile is still detectable; nevertheless, an offset in observed even after rigid-body motion corrections were applied, confirming the behavior of the DIC system described in other studies [71]. To finish, the vibration levels characterizing the railroad service environment can affect the quality of the DIC measurements, but by designing dedicated vibration control solutions it is possible to reduce their effect on the cameras and achieve DIC measurements comparable with those performed in static conditions. It also should be noted that the vibration isolation system presented in this paragraph is intended for proving its feasibility only and that even better results can be obtained with a well-optimized system.

6 - Conclusions

In this study, a novel system based on a 3D digital image correlation (DIC) measurement technique for the measurement of tie deflection profiles and ballast support assessment is proposed and the measurement sensing feasibility is verified experimentally. This research contributes to the overarching goal of developing a SHM monitoring system that can accurately monitor the condition of railway ties and ballast support while trains are in operation to identify defects or damage before they become failures. The high-rate and non-contacting nature of the optical measurement approach lends itself to automated recording allowing for more frequent and cost-effective measurements of track conditions. Unlike most of the conventional SHM sensing systems (e.g. strain gages and accelerometers), which have limitation due to wires, data transmission, power requirements, and only being able to provide discrete sensing, the proposed imaging system allows for full-field displacement measurements over the entire length of the tie-ballast area. Measurements made while

using a projected pattern have been shown to be equivalent to a DIC pattern that is painted on the railway tie. In an extensive series of laboratory tests, the 3D DIC system has been shown to be able to detect out-of-plane displacement as low as 10^{-4} m and with error of nearly 3% when compared with a traditional wired, high-accuracy LVDT. Additionally, the system has been shown to extract the full-field displacement of the tie and can reveal differences in the deflection profiles as various ballast conditions are simulated.

Even more accurate results can be obtained by using higher resolution cameras (e.g. 12 Megapixels) and high-speed sensors can be developed to perform measurements at full-speed operating conditions. To achieve these goals, sets of camera pairs to observe a pattern projected on the track railway tie could be located close to the rail car wheels (i.e. loaded condition) and another pair could be located relatively close away from the wheels (i.e. unloaded condition). Appropriate triggering of the cameras would have to be addressed to synchronize images between camera pairs as a function of train speed and crosstie position. Further development of the concept may bring to use the optically measured deflection profiles to predict induced stress/strain associated with concrete ties, and to assess/classify ballast support conditions using the stress/strain predictions obtained [72]. It is expected that a fully developed system would be able to measure the relative tie deflections, both inside and outside the rail area, with a resolution of approximately 5 microns. The recorded images can be coupled to a finite element model of the crosstie to predict full-field tie stress and strain to identify the ballast support conditions helping to increase railway safety and reduce cost for condition based maintenance.

Funding

This research did not receive any specific grant from funding agencies in the public, commercial, or not-for-profit sectors.

References

1. American Society of Civil Engineers (ASCE). *2013 Report Card for America's Infrastructure, Rail*. http://www.infrastructurereportcard.org/a/#p/rail/overview. (2013, accessed July 2016).
2. Federal Railroad Administration (FRA). *Safety Statistics Data.* http://safetydata.fra.dot.gov (2005-2015, accessed July 2016).
3. Wu H and Wilson N. Railway Vehicle Derailment and Prevention. In: Iwnicki S (ed). *Handbook of railway vehicle dynamics.* New York, CRC press, 2006, pp. 209-238.
4. Hay WW. Cap. 21 – Ballast. In: *Railroad Engineering*. 2nd ed. New York: John Wiley and Sons, 1982, pp. 393-399.
5. Selig ET and Waters JM. *Track geotechnology and substructure management.* 3rd ed. London: Thomas Telford, 2000.
6. Lotfy I, Farhat M, Issa MA et al. Flexural behavior of high-density polyethylene railroad crossties. *Proceedings of the Institution of Mechanical Engineers, Part F: Journal of Rail and Rapid Transit*. 2015; 230(3): 813-824.
7. Qian Y, Tutumluer E, Hashash YMA et al. Effects of Ballast Degradation on Shear Strength Behavior from Large-scale Triaxial Tests. In: *Pan American Conference on Soil Mechanics and Geotechnical Engineering*, Buenos Aires, Argentina, 15–18 November 2015, pp. 1-10, IOS Press.
8. Schafer DH and Barkan CPL. A prediction model for broken rails and an analysis of their economic impact. In: *AREMA annual conference*, Salt Lake City, UT, 21-24 September 2008. Maryland: AREMA.
9. Taylor R. A system for broken rail detection independent of the signaling system. In: IRSE Australasia Technical Meeting, Sydney, Australia, 18 March 2011.
10. Zeman JC, Edwards JR, Barkan CP et al. Failure mode and effect analysis of concrete ties in North America. In *9th International Heavy Haul Conference*, Shanghai, China, 22-25 June, 2011, pp. 270-278, Beijing: China Railway Publishing House.
11. Yu H, Jeong D, Marquis B et al. Railroad Concrete Tie Failure Modes and Research Needs. In: *TRB 94th Annual Meeting*, Washington, DC, 11-15 January, 2015, Paper #15-0311, p. 14. Washington: TRB.
12. Sahu S and Thaulow N. Delayed ettringite formation in Swedish concrete railroad ties. *Cem. Concr. Res*. 2004; 34(9): 1675-1681.
13. Dominguez N, Brancherie D, Davenne L, et al. Prediction of crack pattern distribution in reinforced concrete by coupling a strong discontinuity model of concrete cracking and a bond‐slip of reinforcement model. *Eng. Comp*. 2005; 22(5/6): 558-582.
14. National transportation Safety Board. *Railroad Accident Brief – Metro-North Railroad Derailment*. Report No. NTSB/RAB-14/11, 14 October 2014.
15. Federal Railroad Administration. Broad Agency Announcement, Appendix C – Research Topics, https://www.fra.dot.gov/Page/P0506 (2016, accessed July 2016).
16. Barke D. and Chiu WK. Structural Health Monitoring in the Railway Industry: A Review. *SHM*. 2005; 4(1): 81-93.
17. Johansson A. and Nielsen J. Railway wheel out-of-roundness – Influence of wheel-rail contact forces and track response. In: *13th International Wheelset Conference*, Rome.
18. Askarinejad H, Dhanasekar M and Cole C. Assessing the effects of track input on the response of insulated rail joints using field experiments. *J. Rail and Rapid Transit.* 2012; 227(2): 176-187.
19. Scheppe AJ, Edwards JR, Dersch MS et al. Quantifying Lateral Wheel Loading Variation Using Truck Performance Detectors. In: *TRB 94th Annual Meeting*, Washington, DC, 11-15 January, 2015, Paper # 15-0962, p. 14. Washington: TRB.
20. Buggy S, James S, Staines S, et al. Railway track component condition monitoring using optical fibre Bragg grating sensors. *Meas. Sci. Technol*. 2016; 27(5): 055201.
21. Ho TK, Liu SY, Lee KY et al. An investigation of rail condition monitoring by fiber Bragg grating sensors. *HKIE Transactions*.2009; 16(2): 9-15.

22. Stone DH, Lonsdale C and Kalay S. Effect of wheel impact loading on shattered rims. In: *13th International Wheelset Conference*, Rome.
23. Stark TD and Wilk ST. Monitoring crosstie behavior and crosstie/ballast interaction. *2014 International Crosstie and Fastening System Conference*, 3-5 June, 2014, Urbana, IL.
24. Park K, Kim S, Park H, Lee K. The determination of bridge displacement using measured acceleration. *Eng. Struc.* 2005; 27(3): 371-378.
25. Ramkow-Pedersen O. and Danneskiold-Samsøe U. New on-line wheel tread defect monitoring system with built-in diagnosis facilities. In: *13th International Wheelset Conference*, Rome.
26. Cremins M, Shuai Q, Xu J, et al. Fault detection in railway track using piezoelectric impedance. In: *SPIE Smart Structures and Materials+Nondestructive Evaluation and Health Monitoring*, San Diego, CA, 9-13 March 2014, pp. 90612. International Society for Optics and Photonics.
27. Park S, Inman D and Yun C. An outlier analysis of MFC-based impedance sensing data for wireless structural health monitoring of railroad tracks. *Eng. Struc*. 2008; 30(10): 2792-2799.
28. Hoult N, Bennett PJ, Stoianov I, et al. Wireless sensor networks: creating 'smart infrastructure'. *Proceedings of the ICE-Civil Engineering*, 2009; 162(3): 136-143.
29. Wolfs P, Bleakley S, Senini ST et al. An autonomous, low cost, distributed method for observing vehicle track interactions. In: *Proceedings of IEEE/ASME Joint Rail Conference*, Atlanta, GA, 4-6 April 2006, pp. 279–286.
30. Aw E. *Low cost monitoring system to diagnose problematic rail bed: case study of mud pumping site.* Ph.D. dissertation, MIT, MA, 2007.
31. Reason J, Chen H, Crepaldi R et al. Intelligent Telemetry for Freight Trains," in Phan T, Montanari R and Zerfos P (eds.) *Mobile Computing, Applications, Services*, vol. 35. Berlin: Springer-Verlag, 2010, pp. 72–91.
32. Hodge V, O'Keefe S, Weeks M et al. Wireless Sensor Networks for Condition Monitoring in the Railway Industry: A Survey. *IEEE Trans Intell Transport Syst.* 2015; 16(3): 1088-1106.
33. Greene R, Yates JA and Patterson EA. Crack detection in rail using infrared methods. *Opt. Eng*. 2007; 46(5): 051013.
34. Wilson J, Tian G, Mukriz I, et al. PEC thermography for imaging multiple cracks from rolling contact fatigue. *NDT & E Int*. 2011; 44(6): 505-512.
35. Lanza di Scalea F. Ultrasonic Testing Applications in the Railroad Industry. In Moore PO (ed.) *Special Applications of Ultrasonic Testing, Non-destructive Testing Handbook*, 3rd edition. Columbus: American Society for Nondestructive Testing, 2007, pp. 535-540.
36. National transportation Safety Board. *Railroad Accident Brief – Derailment of CSX Transportation Train No. Q39010*. Report No. NTSB/RAB-08/05, 8 May 2007.
37. Ph Papaelias M, Roberts C, Davis C. A review on non-destructive evaluation of rails: state-of-the-art and future development. *Proceedings of the Institution of Mechanical Engineers, Part F: Journal of Rail and Rapid Transit.* 2008; 222(4): 367-384.
38. Coccia S, Phillips R, Nucera C et al. UCSD/FRA non-contact ultrasonic guided-wave system for rail inspection: an update. In: *SPIE Smart Structures and Materials+Nondestructive Evaluation and Health Monitoring*, San Diego, CA, 25-29 March 2011, pp. 798113. International Society for Optics and Photonics.
39. Olhoeft GR and Selig ET. Ground-penetrating radar evaluation of railway track substructure conditions. In: *9th International Conference GPR2002*, Santa Barbara, CA, 29 April – 2 May 2002, pp. 48-53. International Society for Optics and Photonics.
40. Federal Railroad Administration. *Ground Penetrating Radar for Railroad Track Substructure Evaluation.* Report No. FRA/ORD-05/04, 5 April 2005.
41. Molina LF, Resendiz E, Edwards JR et al. Condition monitoring of railway turnouts and other track components using machine vision. In: *TRB 90th Annual Meeting*, Washington, DC, 23-27 January, 2011, Paper #11-1442, p. 17. Washington: TRB.
42. Deutschl E, Gasser C, Niel A et al. Defect detection on rail surfaces by a vision based system. In: *Intelligent Vehicles Symposium IEEE*, Parma, Italy, 14-17 June 2004 IEEE, pp. 507-511. IEEE.

43. ENSCO. *Rail Surface and Wear Condition Measurement Systems, Rail Profile Measurement Systems - Non-contact, completely digital, optical imaging technology improves performance of rail gage measurement*. http://www.ensco.com/products-services/rail-technologies/track-inspection -systems/rail-surface-wear-condition.htm. (2011, accessed July 2016).
44. ENSCO. *Autonomous Inspection Systems - Track assessment monitoring and maintenance systems for safe and reliable operation*. http://www.ensco.com/products-services/rail-technologies/track-inspection-systems/autonomous-inspection-systems.htm. (2011, accessed July 2016).
45. Ruvo P, Ruvo G, Distante A et al. A Visual Inspection System for Rail Detection and Tracking in Real Time Railway Maintenance. *TOCSJ*. 2008; 2(1): 57-67.
46. Bowness D, Lock A, Powrie W et al. Monitoring the dynamic displacements of railway track. *Proceedings of the Institution of Mechanical Engineers, Part F: Journal of Rail and Rapid Transit.* 2007; 221(1): 13-22.
47. Murray C, Take W, Hoult N. Measurement of vertical and longitudinal rail displacements using digital image correlation. *Canadian Geotechnical Journal*. 2015; 52(2): 141-155.
48. Clark R. Rail flaw detection: overview and needs for future developments. *NDT & E International*. 2004; 37(2): 111-118.
49. Rizzo P. Sensing solutions for assessing and monitoring railroad tracks. In Wang ML, Lynch JP and Sohn H (eds.) *Sensor Technologies for Civil Infrastructures - Volume 2: Applications in Structural Health Monitoring*. 1st ed. New York: Elsevier, 2014, pp. 497-524.
50. Sutton MA, Orteu JJ and Schreier HW. Image correlation for shape, motion and deformation measurement. Basic concepts, theory and applications. 1st ed. New York City, NY: Springer, 2009, p. 321.
51. Luo PF, Chao YJ, Sutton AM et al. Accurate measurement of three-dimensional deformations in deformable and rigid bodies using computer vision. Exp. Mech. 1993; 33(2), 123-132.
52. Schmidt T, Tyson J, Galanulis K. Full-Field Dynamic Displacement and Strain Measurement Using Advanced 3D Image Correlation Photogrammetry: Part I. *Exp Tech*. 2003; 27(3): 47-50.
53. Peters WH, Ranson WF, Sutton MA et al. Application of Digital Image Correlation Methods to Rigid Body Mechanics. *Opt. Eng.* 1983; 22(6):738-42.
54. Chu TC, Ranson WF and Sutton MA. Applications of Digital Image Correlation Techniques to Experimental Mechanics. *Exp. Mech.* 1985; 25(3): 232-244.1985.
55. Kahn-Jetter ZL and Chu TC. Three-Dimensional Displacement Measurements Using Digital Image Correlation and Photogrammic Analysis. *Exp. Mech*. 1990; 30(1): 10–16.
56. Schmidt T, Tyson J, Galanulis K. Full-Field Dynamic Displacement and Strain Measurement Using Advanced 3D Image Correlation Photogrammetry: Part II. *Exp Tech*. 2003; 27(4): 22-26.
57. Yoneyama S, Kitagawa A, Iwata S, Tani K, Kikuta H. Bridge deflection measurement using Digital Image Correlation. *Exp Tech.* 2007; 31(1): 34-40.
58. LeBlanc B, Niezrecki C, Avitabile P et al. Damage detection and full surface characterization of a wind turbine blade using three-dimensional digital image correlation. *SHM*. 2013; 12(5-6): 430-439.
59. Lundstrom T, Baqersad J, Niezrecki C. Monitoring the Dynamics of a Helicopter Main Rotor With High-Speed Stereophotogrammetry. *Exp Tech.* 2016; 40(3): 907-919.
60. Asl M, Niezrecki C, Sherwood J et al. Similitude Analysis of the Strain Field for Loaded Composite I-Beams Emulating Wind Turbine Blades. In ASFC, Williamsburg, VA, 19-22 September, 2016, in press.
61. American Railway Engineering and Maintenance-of-Way Association. Manual for Railway Engineering, Chapter 30.4: Concrete Ties, 2016.
62. Baumer. *FWX20C NeuroCheck Edition – Digital Color Progressive Scan Camera*. http://rhengineering.de/wp-content/uploads/2015/07/Baumer_FWX20c_NC_v10e_041013.pdf (2015, accessed July 2016).
63. Nonis C. *Structural Health Monitoring Of Bridges Using Three-Dimensional Digital Image Correlation.* MS thesis, University of Massachusetts Lowell, 2013.
64. Poozesh P, Baqersad J, Niezrecki C et al. A multi-camera stereo DIC system for extracting operating mode shapes of large scale structures. *Advancement of Optical Methods in Experimental Mechanics*. 2016; 3: 225-238.

65. Sabato A and Niezrecki C. Full-scale damage detection of railroad crossties using Digital Image Correlation. In *iDICs 2016*, Philadelphia, PA, 7-10 November 2016, in press.
66. Sabato A, Beale CH and Niezrecki. A Novel Optical Investigation Technique for Railroad Track Inspection and Assessment. Accepted to *SPIE Smart Structures and Materials+ Nondestructive Evaluation and Health Monitoring.* Portland, OR, 25-29 March 2017. International Society for Optics and Photonics.
67. Pan B, Wu D, and Xia Y. An active imaging digital image correlation method for deformation measurement insensitive to ambient light. *Optics & Laser Tech.* 2012; 44(1): 204-209.
68. Kerr AD. *Fundamentals of Railway track engineering*, 1st ed. Omaha, NE: Simmons-Boardman Books Inc., 2003, p. 393.
69. Lutch RH, Harris DK and Ahlborn TM. Prestressed concrete ties in North America. In: AREMA annual conference and exposition, Chicago, IL, 20-23 September 2009. AREMA.
70. Chen Z, Shin M, Andrawes B et al. Parametric study on damage and load demand of prestressed concrete crosstie and fastening systems. *Engineering Failure Analysis.* 2014; 46: 49-61.
71. Balcaen R, Reui PL, Lava P et al. Evaluation of Camera Motion in Stereo-DIC, in iDICs. Philadelphia, PA, 7-10 November, 2016.
72. Yu H. Estimating Deterioration in the Concrete Tie-Ballast Interface Based on Vertical Tie Deflection Profile: A Numerical Study. In: *2016 Joint Rail Conference*, Columbia, SC, 12-15 April 2016, paper no. JRC2016-5783, pp. V001T01A024. New York: ASME.